Coherent THz wave emission from HgTe quantum dots

Thibault Apretna, Niloufar Nilforoushan, Jérôme Tignon, Sukhdeep Dhillon, Francesca Carosella, Robson Ferreira, E. Lhuillier, Juliette Mangeney

▶ **To cite this version:**

Thibault Apretna, Niloufar Nilforoushan, Jérôme Tignon, Sukhdeep Dhillon, Francesca Carosella, et al.. Coherent THz wave emission from HgTe quantum dots. Applied Physics Letters, 2022, 121 (25), pp.251101. 10.1063/5.0134396 . hal-03941198

HAL Id: hal-03941198
https://hal.science/hal-03941198v1

Submitted on 24 Apr 2024

HAL is a multi-disciplinary open access archive for the deposit and dissemination of scientific research documents, whether they are published or not. The documents may come from teaching and research institutions in France or abroad, or from public or private research centers.

L'archive ouverte pluridisciplinaire **HAL**, est destinée au dépôt et à la diffusion de documents scientifiques de niveau recherche, publiés ou non, émanant des établissements d'enseignement et de recherche français ou étrangers, des laboratoires publics ou privés.

Coherent THz Wave Emission from HgTe Quantum Dots

T. Apretna[1], N. Nilforoushan[1], J. Tignon[1], S. Dhillon[1], F. Carosella[1], R. Ferreira[1], E. Lhuillier[2], J. Mangeney[1*]

[1]*Laboratoire de Physique de l'Ecole Normale Supérieure, ENS, Université PSL, CNRS, Sorbonne Université, Université Paris-Diderot, Sorbonne Paris Cité, Paris, France*

[2]*Sorbonne Université, CNRS, Institut des NanoSciences de Paris, 4 place Jussieu, 75005 Paris France*

**juliette.mangeney@phys.ens.fr*

Mercury Telluride (HgTe) nanocrystal (NC) quantum dots are very promising for THz technology as they exhibit broad THz absorption resonances and a carrier lifetime of a few picoseconds, as well as being easily fabricated using solution synthesis. In this work, we show their light emission properties in the THz spectral range, up until now unexplored, and show how THz pulse generation can be used for microscopic insights into these NCs. In particular, we report on coherent THz emission from large HgTe NCs excited by linearly-polarized optical pulses, via second-order nonlinear effects. The peak emission frequency is tunable from 0.4 to 0.8 THz by varying the incident angles of the optical pulses from 0° to 45°. Our results reveal that the THz emission is induced by transient photocurrents arising from both photogalvanic and photon drag effects. By pushing the light emission of colloidal quantum dots down to the THz spectral range, our study expands the application fields of nanocrystals, especially towards the development of easily integrable and tunable THz emitters and quantum THz devices.

Terahertz (THz) emission spectroscopy, based on coherent THz emission from materials excited by ultrashort optical pulses, is a very powerful tool to probe the ultrafast dynamics of current generation in materials.[1] Previous works have reported, for example, coherent THz emission induced by ultrafast photogalvanic and photon drag in topological materials [2,3] and Weyl semimetals,[4,5] photon drag effects in graphene[6,7,8] and 2D materials,[9] surface-plasmon-enhanced optical rectification in graphene,[10] ultrafast injection and shift photocurrents in hybrid perovskites,[11,12] ultrafast spin current in spintronic structures,[13,14] photo-Dember field and surface depletion field in bulk semiconductors.[15,16,17] Each of these permits microscopic insights into the carrier generation and transport in their corresponding materials. Also, the study of THz emission properties from materials excited by ultrashort optical pulses plays an important role in the development of advanced THz sources such as recently demonstrated spintronic emitters that have considerably impacted the domain. [13] HgTe nanocrystals (NCs) of large size, typically a few tens of nanometers, are emerging quantum dots with great potential for THz technology. Indeed, rapid progress on the colloidal growth of large HgTe NCs (up to 1 µm) has made it possible to demonstrate a broad and tunable intraband absorption at THz frequencies.[18,19,20] This strong intraband absorption in the THz spectral range

originates from multiple intraband transitions of single carriers between the quantized states of self-doped HgTe NCs.[21,22,23] Also, carrier lifetimes of few picoseconds have been recently reported in these large HgTe NCs.[23,24] While THz electroluminescence and even stimulated THz emission from CdHgTe/HgTe quantum wells has been demonstrated previously [25,26], coherent THz wave emission from large HgTe quantum dots excited by femtosecond optical pulses, and more generally from any quantum dots, remains unexplored to date.

Here, we use THz emission spectroscopy to demonstrate coherent THz emission from a film of large HgTe NCs excited by femtosecond optical pulses at room temperature. We experimentally study the properties of emission with respect to the incident and polarization angles of the linearly-polarized optical pulses. We show a frequency tuning of the THz emission from 0.4 to 0.8 THz controlled by the incident angle of the optical pulses. Our analysis of experimental features reveals that the radiated THz emission, which has a dominant component in the direction normal to the surface of the HgTe NCs film, results from transient second-order nonlinear currents driven by both photogalvanic and photon drag effects.

The HgTe NCs are grown by the simultaneous injection of mercury chloride and trioctylphosphine telluride in hot (300 °C) oleylamine, used as coordinating solvent.[18] After reaction quenching, the particles are cleaned and capped with 1-dodecanethiol ligands. These insulating long-chain organic ligands surrounded each HgTe NC strongly limit the carrier hopping between neighboring nanocrystals. The typical sizes of the HgTe NCs are large according to electronic microscopy (see Figure 1(a)) and X-ray diffraction (XRD) (see Supplementary Figure S1). From the X-ray diffraction line width and using the Debye–Scherrer equation, we estimate a mean size of the NCs of L≈90 nm, which is consistent with the small particles observed by electronic microscopy and suggests that the largest NCs are polycrystalline. The HgTe NCs film, of 13 µm-thick, is then deposited on a 500 µm-thick quartz substrate, which is transparent in the optical and low-frequency THz spectral range. The absorbance spectrum of the HgTe NCs film, shown in Figure 1(b), exhibits a broad resonance at low frequency centered at ≈4.5 THz, assigned to multiple intraband transitions of single carriers between the quantized states of the HgTe NCs, and a broad absorption at high frequency (>30 THz) arising from interband transitions [23]. The narrow absorption feature observed at 3.6 THz is attributed to the additional transverse optical (TO) phonon absorption.

The THz time-domain emission spectroscopy system used to investigate the coherent THz radiation emitted from the HgTe NCs film is based on a mode-locked Ti:Saphir laser operating at 80 MHz and delivering 15 fs optical pulses with a central wavelength of 800 nm. The optical pulses are focused onto the HgTe NCs film with a typical beam size of 200 µm. The incidence angle, θ_{in}, of the optical excitation onto the HgTe NCs film is controlled by a movable mirror positioned in front of

the sample (see Figure 1(c)). The incident angle of the optical pulses inside the HgTe NCs film, θ, is deduced from Snell's Law using $\theta = \arcsin(\sin(\theta_{in})/n_{opt})$ with $n_{opt} = 2.35$, the refractive index of the HgTe NCs film at optical frequencies.[27] The optical pulses are linearly polarized in the (x,y) plane and a half-wave plate is used to fix the optical electric field orientation along a variable angle α (with respect to the x-axis, see Figure 1(d)). The coherent THz radiation emitted from the HgTe NCs film is detected in a transmission mode using off-axis parabolic mirrors and a conventional electro-optic detection technique based on a 2 mm-thick (110) ZnTe crystal (see Figure 1(c)).[28] In a default experimental configuration, the electro-optic probe detects the component of $E_{THz}(t)$ along the h-axis, E_{THz}^{h} (see Figure 1(d)). The detection angle of the emitted THz radiation, Φ_{det}, is adjusted by changing the orientation of the HgTe NCs sample with respect to the Y axis, with XYZ representing the HgTe NCs sample coordinate framework. Since electro-optic detection technique is only sensitive to THz radiation synchronized with the femtosecond pulses, the incoherent thermal background is suppressed. All measurements are performed at room temperature.

Figure 1(e) shows typical THz waveform, $E_{THz}(t)$, emitted by the HgTe NCs film excited by p-polarized optical pulses incident at $\theta_{in} = 45°$ and detected at $\Phi_{det} = 45°$. The observed THz waveform is mainly unipolar with a positive peak whose full-width-at-half-maximum is 230 fs. Note that the THz emission occurs on a much shorter time scale than photocarrier thermalization (involving intraband carrier–carrier and electron–optical phonon scattering) which occurs over ≈2 ps, so it is not related to photoluminescence.[23] The amplitude spectrum, obtained by the Fourier transform of the temporal electric field waveform, consists of a single broad peak centered at 0.7 THz, as shown in Figure 1(f) (black solid curve). The spectrum of the measured THz emission is not limited by the bandwidth of our electro-optic detection system, which extends up to >3 THz, as shown by the amplitude spectrum measured with a low-temperature-grown GaAs photoconductive antenna as emitter and a substrate of quartz in place of the sample (red dashed curve in Figure 1(f)).

FIG 1. (a) Scanning electron microscopy image of large HgTe NCs (see Ref [23]). (b) Absorbance spectra of the HgTe NCs film obtained by THz TDS (black solid line) and FTIR (green solid line) measurements. (c) Schematic illustration of experimental setup and (d) THz emission in a transmission mode. xyz, XYZ and nhv represent the laboratory, sample and detector coordinate framework, respectively. The p-polarized and s-polarized optical excitations are along the x-axis and y-axis, respectively. (e) Experimental electric field waveform and its associated spectrum (f) emitted by large HgTe NCs film illuminated by p-polarized femtosecond optical pulses ($\theta_{in} = 45°$ and $\Phi_{det} = 45°$). The red dashed line is a reference amplitude spectrum measured with a low-temperature-grown GaAs photoconductive antenna as emitter and a substrate of quartz in place of the sample.

To get insight on the ultrafast currents underlying the THz radiation, we probe the dependence of the THz radiation emitted from the HgTe NCs film on the incident optical fluence, the incidence and detection angles for p-polarized optical pulses. We observe in Figure 2(a) that the peak-to-peak THz electric field, E_{pp}, scales linearly with the excitation fluence and thus quadratically with the incident optical electric field. The electric field amplitude reaches ≈1.5% of that radiated by a large-area interdigitated low-temperature-grown GaAs photoconductive antenna.[29] The shape of the electric field waveforms and therefore of the amplitude spectra remains essentially constant for all optical fluences. Figure 2(b) shows a reverse polarity of the time-oscillations for both opposite incidence and detection angles, $\theta_{in} = 30°$, $\Phi_{det} = 30°$ (green solid curve) and $\theta_{in} = -30°$,$\Phi_{det} = -30°$ (black solid curve). In contrast, holding constant the detection angle Φ_{det}, the waveforms do show no reverse polarity for opposite incident angle $\theta_{in} = \pm 15°$, but a large variation of their amplitude (see Figure 2(c)). By varying the detection angle Φ_{det} and keeping θ_{in} constant, we observe that the THz electric field amplitude reaches a maximum at Φ_{det}=30°, as shown in Figure 2(d), and also opposite sign of the waveform for opposite detection angles $\Phi_{det} = \pm 15°$. Note that no THz emission is recorded at $\theta_{in} = 0°$ and $\Phi_{det} = 0°$. All these features reveal that the THz radiation originates from transient currents with several spatial components, with a dominant component along the normal to the surface of the HgTe NCs film (along Z in Figure 1(d)). We further characterize the polarization state of the THz electric field on the electro-optic detector using a grid THz polarizer. Figure 2(e) shows that the component of E_{THz} along h-axis, E_{THz}^{h}, is x3.8 times larger in amplitude than the component along v-axis, E_{THz}^{v}, for p-polarized incident optical pulses, $\theta_{in} = 45°$ and $\Phi_{det} = 45°$. To determine the polarization state of the THz electric field emitted in the HgTe NCs film, we first calibrate the birefringence introduced by a similar bare 500 µm-thick quartz substrate in the same geometry, $\theta_{in} = 45°$ and $\Phi_{det} = 45°$. We then calculate the THz electric field vector after its passage through the birefringent quartz substrate assuming that the THz emission at the output of the HgTe NCs film is fully polarized along the h-axis (E_{THz}^{v}=0). The calculated component E_{THz}^{v} (dashed red line) relatively well reproduces the measured E_{THz}^{v}, small deviation is attributed to uncertainty in the absolute orientation of the quartz substrate onto the sample holders. This observation indicates that, for p-polarized optical excitation, the emitted THz radiation is orientated along the h-axis (*i.e.* p-polarized) and that the measured component E_{THz}^{v} essentially results from the birefringence of the quartz substrate. Also, we probe the dependance of the THz radiation on the polarization angle of the optical pulses, α, and observe a small variation in the amplitude spectra from p-polarized to s-polarized optical pulses as shown in Figure 2(f).

FIG 2 (a) The peak-to-peak THz electric field as a function of the optical fluence incident on the HgTe NCs film. The red squares are the experimental data, and the error bars show the standard deviation associated with noise fluctuations. The dashed line underlines the linear dependence. (b) Time-resolved electric field profiles measured for both opposite incidence and detection angles, $\theta_{in} = 30°$, $\Phi_{det} = 30°$ (green solid curve) and $\theta_{in} = -30°$,$\Phi_{det} = -30°$ (black solid curve) under p-polarized optical excitation. (c) Time-resolved electric field profiles measured for $\theta_{in} = \pm 15°$ and $\Phi_{det} = 15°$ under p-polarized optical excitation. Curves are shifted vertically for clarity. (d) Time-resolved electric field profiles measured for different Φ_{det} under p-polarized optical excitation incident at $\theta_{in} = 15°$. Curves are shifted vertically for clarity. (e) Electric field waveforms excited by p-polarized optical pulses and detected along the h-direction and v-direction on the electro-optic detector and their associated spectrum (insert). The red dashed curve represents the calculated amplitude spectrum. (f) Amplitude spectra of the THz electric field emitted by HgTe NCs films under p-polarized (black solid curve) and s-polarized (red solid curve) excitation for $\theta_{in} = 30°$ and $\Phi_{det} = 30°$ and $\theta_{in} = 45°$ and $\Phi_{det} = 45°$.

We now examine the potential mechanisms responsible for the observed coherent THz emission from optically excited HgTe NCs film, which evolves linearly with the optical pulse fluence. Coherent THz emission from material systems excited by femtosecond optical pulses are mainly due to ultrafast charge transports and/or nonlinear optical effects. Charge currents resulting from the acceleration of photogenerated carriers by surface built-in field formed by either band bending at the surface, or by the photon-Dember effect which implies formation of a dipole due to a mobility difference between electrons and holes, are along a direction normal to the material surface.[9] However, these ultrafast currents can be ruled out in HgTe NCs film due to the confinement of carriers inside each NC. Indeed, transport in HgTe NCs films occurs though hopping typically toward nearest neighbor at room temperature, with a hopping time τ_{hop}, given by $\tau_{hop} = \frac{eR^2}{6\mu k_b T}$ with e the proton charge, R the particle radius, μ the carrier mobility and k_bT the thermal energy.[30,] If we assume a typical value of μ=10-2 $cm^2.V^{-1}.s^{-1}$ for the mobility, this leads to $\tau_{hop} = 16\,ns$, a time scale much longer than the relaxation mechanism under consideration here. This it is reasonable to assume that all processes are intraparticle process.[31] Therefore, the observed coherent THz emission is attributed to second-order nonlinear effects.[32,33,34,35] In general, the second-order nonlinear current density induced at the difference frequency by an electromagnetic wave with a complex electric field component $\overrightarrow{E_{opt}}(\vec{q},\omega)$ is phenomenologically described by: $j_\lambda^{(2)}(\vec{q}) = \sum_\nu \sum_\eta \sigma_{\lambda\nu\eta}(\vec{q},\omega) E_\nu(\vec{q},\omega) E_\eta^*(\vec{q},\omega)$, where $\sigma_{\lambda\nu\eta}(\vec{q})$ is the photocurrent conductivity tensor, the indices run through the three spatial coordinates X,Y and Z, $\vec{q}$ is the optical wavevector, and ω is the optical photon frequency. The tensor $\sigma_{\lambda\nu\eta}(\vec{q})$ incorporates the microscopic properties of the material, and in our case, represents an average value of the ensemble of the HgTe NCs arranged in the film. Indeed, as the HgTe NCs are randomly oriented and their sizes (≈90 nm) are much

smaller than both the optical beam size on the film (≈200 μm) and the optical and THz wavelengths, the HgTe NCs film is considered optically isotropic in the plane (X,Y). Expanding the second-order conductivity $\sigma_{\lambda\nu\eta}(\vec{q})$ to linear order in $\vec{q}$ gives $\sigma_{\lambda\nu\eta}(\vec{q}) = \left[\chi_{\lambda\nu\eta} + \sum_\mu T_{\lambda\mu\nu\eta}\, q_\mu\right]$. The first term represents photogalvanic effects, which originates from the spatial charge transfer during the transition from valence band to conduction band in non-centrosymmetric materials, whereas the second term describes the photon drag effect, which arises from the transfer of linear momentum from the incident photons to the excited electrons.[36] In our experimental configuration, the optical pulses propagate in the (XZ) plane with $\vec{q} = q_0(\sin\theta\,, 0, -\cos\theta)$ and the electrical vectors of the optical pulses, incident on the HgTe NCs film, are linearly polarized. Therefore, $\sigma_{\lambda\nu\eta}(\vec{q})$ is symmetrical with regards to spatial coordinate index ν and η, leading to $\sigma_{\lambda\nu\eta}(\vec{q}) = \sigma_{\lambda\eta\nu}(\vec{q})$.[32] In the sample coordinate system, $\vec{E}_{opt} = E_0 \cos\alpha \cos\theta\, \vec{X} - E_0 \sin\alpha\, \vec{Y} + E_0 \sin\theta \cos\alpha\, \vec{Z}$, yielding to: $j_\lambda^{(2)}(\theta,\alpha) = j_{\lambda 0}(\theta) + j_{\lambda C}(\theta)\cos 2\alpha + j_{\lambda S}(\theta)\sin 2\alpha$, (see details in the Supplementary). The symmetry argument related to the optical isotropy of the film in the plane (X,Y) yields to the equivalence of all in-plane directions. On the other hand, there is no equivalence of Z and -Z directions because the HgTe NCs film is deposited on a substrate. Thus, the components of the total second-order nonlinear current density, for p-polarized optical pulses ($\alpha = 0$), can be simplified into the form (details of the calculations can be found in Supplementary):

$$j_X^{(2)}(\theta) = {E_0}^2[\chi_{XXZ}\sin 2\theta + q_0(T_{XXZZ}+2T_{XZXZ} - T_{XXXX})sin^3\theta + q_0(T_{XXXX} - 2T_{XZXZ})\sin\theta]$$

$$j_Y^{(2)}(\theta) = 0$$

$$j_Z^{(2)}(\vec{\theta}) = {E_0}^2[\chi_{ZXX} + (\chi_{ZXX} - \chi_{ZZZ})sin^2\theta + q_0\,(2T_{ZXZX} + T_{ZZZZ})\cos\theta + q_0(T_{ZZZZ} - T_{ZZXX} - 2T_{ZXXZ})\cos^3\theta]$$

The far field THz electric field component along h-axis on the electro-optic detector is expressed as:

$$E_{THz}^h \propto {E_0}^2[A + B\cos\theta + C\sin\theta + \mathrm{D}\sin 2\theta + \mathrm{E}\cos^3\theta] \qquad (1)$$

with A=$-\sin\Phi_{in}\,(2\chi_{ZXX})$, B=$-\sin\Phi_{in}\,q_0(2T_{ZXZX} + T_{ZZZZ})$, C=$\cos\Phi_{in}\,q_0(T_{XXXX} - 2T_{XZXZ})$, $D = \cos\Phi_{in}\,\chi_{XXZ}$, E=$-\sin\Phi_{in}\,q_0(T_{ZZZZ} - T_{ZZXX} - 2T_{ZXXZ})$, where Φ_{in} corresponds to the internal angle of the THz radiation in the HgTe NCs film. It is linked to Φ_{det} and Φ_{quartz} (the angle of the THz radiation in the quartz substrate) through the Snell's law $\sin\Phi_{in} = (n_{quartz}/n_{film})\sin\Phi_{quartz}$ and $\sin\Phi_{quartz} = {n_{quartz}}^{-1}\sin\Phi_{det}$. Terms in $sin^2\theta$ and $sin^3\theta$ have been neglected since the maximum incident angle $|\theta_{in}| = 75°$ corresponds to a much smaller internal angle $|\theta| = 24°$ in the HgTe NCs film. The coefficients A, D are related to photogalvanic effects while B, C, E are related to photon drag effects, and all are mean

values over all frequencies. To get insight into the relative contributions of photogalvanic and photon drag currents underlying the THz radiation emitted by the HgTe NCs, we measure the emitted THz waveforms as a function of θ_{in}. We observe an increase of the THz waveform amplitude and a decrease of the full-width-at-half-maximum of the THz waveforms as θ_{in} rises to 45° and, for larger values of θ_{in}, these tends reverse (see Figure 3(a)). These tendencies result in a shift of the THz spectra in the range 0.4-0.8 THz by varying θ_{in}, as shown in Figure 3(b), leading to a tunability of the emitted THz radiation of $\Delta\omega/\omega$=50%. Such an optically controlled spectral tunability is not achievable in conventional THz emitters. Figure 3(c) shows that the peak-to-peak THz electric field exhibits a strong dependence with θ and remains positive even at negative incident angle. This experimental trend is well fitted with the expression of E_{THz}^{h} (red dashed curve). Moreover, the expression of E_{THz}^{h} (equation (1)) well explains the other dependencies of the measured THz emission. Indeed, calculation predicts that $E_{THz}^{h}(-\Phi_{det}, -\theta) = -E_{THz}^{h}(\Phi_{det},\theta)$, which is consistent with the reverse polarity observed experimentally in Figure 2(b). For a constant detection angle Φ_{det} but an opposite incident angle θ_{in}, E_{THz}^{h} is reduced due to odd terms in θ_{in} in the sum. Also, E_{THz}^{h} is predicted to cancel for $\theta_{in} = 0°$ and $\Phi_{det} = 0°$, as observed experimentally. The component of the emitted THz electric field along v-axis on the electro-optic detector results from birefringence effects in quartz substrate only, as $j_Y^{(2)} = 0$. The weak dependence of the emitted THz radiation on the polarization of the optical pulses (Figure 2(f)) is attributed on the one hand to the small angle of incidence of the optical pulses in the HgTe NCs film (θ of only $17.5°$ for $\theta_{in} = 45°$), which strongly limits the Z-axis component of the optical electric field, and on the other hand to the isotropy of the (X,Y) plane, which makes E_x and E_y equivalent. Importantly, the good agreement between the predicted θ-dependence of E_{THz}^{h} with the experimental data cannot be obtained with a single effect indicating the contribution of both photon drag and photogalvanic effects in the coherent THz emission process. Also, the weight of coefficients involved in $j_X^{(2)}$ are smaller than those involved in $j_Z^{(2)}$revealing that the dominant transient photocurrent is along the direction normal to the HgTe NCs film surface.

FIG 3 (a) Time-resolved electric field profiles and the correspond normalized amplitude spectra (b) measured for different θ_{in} ranging from 0 to 75° under p-polarized optical excitation at $\Phi_{det} = 45°$. (c) The peak-to-peak THz electric field as a function of the incidence angle in the HgTe NCs film, θ. The circles are the experimental data and the red dashed line is the best-fit curve using equation (1). We found A=-377; B=575; C=70; D=-34; E=-197.

In conclusion, using THz emission spectroscopy we have demonstrated THz emission from large HgTe NCs excited by femtosecond optical pulses induced by transient second-order nonlinear photocurrents. We have highlighted the role of photogalvanic and photon drag effects underlying the nonlinear photocurrents and found that their main component is oriented

in the direction normal to the HgTe NCs film. We have also shown the possibility to tune the THz emission in the range 0.4-0.8 THz by changing the incident angle of the optical pulses. The physical origin of this frequency shift remains not clear and would require further investigation to be identified. Our work opens the perspective to study helicity-dependent photocurrents via the circular photogalvanic effect in these HgTe NCs and thus to probe the possible presence of topological surface states [37,38] and their potential to emit chiral THz waves. Also, the investigation of transient photocurrents and coherent THz emission from alternative nanocrystals and quantum dots could provide unique microscopic insights on their properties. This work represents an important step in colloidal quantum dot-based light emitters by extending their spectral range to THz frequencies. It therefore has important implications for THz technology with significant prospects in the development of THz emitters that can be easily integrated on various devices and towards the development of quantum THz devices.

Supplementary Material

See the supplementary material for additional information on sample preparation, material characterization and modelling.

The authors thank C. Flytzanis for fruitful discussions. The project is supported by ERC starting grant blackQD (grant n° 756225) and consolidator grant LEON (grant n° 820133). This work is supported by French state funds managed by the ANR using grant Copin (ANR-19-CE24-0022), Frontal (ANR-19-CE09-0017), Graskop (ANR-19-CE09-0026), NITQuantum (ANR-20-ASTR-0008), Bright (ANR-21-CE24-0012-02), MixDferro (ANR-21-CE09-0029), QuickTera (ANR-22-CE09-0018) and STEM2D (ANR-19-CE24-0015).

The authors declare no conflict of interest

References

[1] X. C. Zhang, D. H. Auston, *J. Appl. Phys.* 71, 326 (1992).

[2] Shunyi Ruan, Xian Lin, Haiyang Chen, Bangju Song, Ye Dai, Xiaona Yan, Zuanming Jin, Guohong Ma, Jianquan Yao, *Appl. Phys. Lett.*, 118, 011102 (2021).

[3] L. Braun, G. Mussler, A. Hruban, M. Konczykowski, T. Schumann, M. Wolf, M. Münzenberg, L. Perfetti, T. Kampfrath, *Nat. Commun*., 7, 13259 (2016).

[4] Y. Gao, S. Kaushik, E. J. Philip, Z. Li, Y. Qin, Y. P. Liu, W. L. Zhang, Y. L. Su, X. Chen, H. Weng, D. E. Kharzeev, M. K. Liu, J. Qi, *Nat. Commun.,* 11**,** 720 (2020).

[5] N. Sirica, R. I. Tobey, L. X. Zhao, G. F. Chen, B. Xu, R. Yang, B. Shen, D. A. Yarotski, P. Bowlan, S. A. Trugman, J.-X. Zhu, Y. M. Dai, A. K. Azad, N. Ni, X. G. Qiu, A. J. Taylor, R. P. Prasankumar, *Phys. Rev. Lett.,* 122, 197401 (2019).

[6] J. Maysonnave, S. Huppert, F. Wang, S. Maero, C. Berger, W. de Heer, T. B. Norris, L. A. De Vaulchier, S. Dhillon, J. Tignon, R. Ferreira, J. Mangeney, *Nano Lett.*, 14, 10, 5797 (2014).

[7] L. Zhu, Y. Huang, Z. Yao, B. Quan, L. Zhang, J. Li, C. Gu, X. Xu, Z. Ren, *Nanoscale*, 9, 10301 (2017).

[8] M.M. Glazov, S.D. Ganichev, *Phys. Reports*, 535, 101 (2014).

[9] Yuanyuan Huang, Zehan Yao, Chuan He, Lipeng Zhu, Longhui Zhang, Jintao Bai, Xinlong Xu, *J. Phys.: Condens. Matter*, 31 153001 (2019).

[10] Young-Mi Bahk, Gopakumar Ramakrishnan, Jongho Choi, Hyelynn Song, Geunchang Choi, Kim, Hyup Yong, Kwang Jun Ahn, Dai-Sik Kim, Paul C. M. Planken, *ACS Nano*, 8, 9089 (2014).

[11] B. Guzelturk, R. A. Belisle, M. D. Smith, K. Bruening, R. Prasanna, Y. Yuan, V. Gopalan, C. J. Tassone, H. I. Karunadasa, M. D. McGehee, A. M. Lindenberg, *Adv. Mater.*, 30, 1704737 (2018).

[12] Petr A. Obraztsov, D. Lyashenko, P. A. Chizhov, K. Konishi, N. Nemoto, M. Kuwata-Gonokami, E. Welch, A. N.Obraztsov, A. Zakhidov, *Commun Phys.*, 1, 14 (2018).

[13] T. Seifert, S. Jaiswal, U. Martens, J. Hannegan, L. Braun, P. Maldonado, F. Freimuth, A. Kronenberg, J. Henrizi, I. Radu, E. Beaurepaire, Y. Mokrousov, P. M. Oppeneer, M. Jourdan, G. Jakob, D. Turchinovich, L. M. Hayden, M. Wolf, M. Münzenberg, M. Kläui, T. Kampfrath, *Nature Photon.*, 10, 483 (2016).

[14] T. H. Dang, J. Hawecker, E. Rongione, G. Baez Flores, D. Q. To, J. C. Rojas-Sanchez, H. Nong, J. Mangeney, J. Tignon, F. Godel, S. Collin, P. Seneor, M. Bibes, A. Fert, M. Anane, J.-M. George, L. Vila, M. Cosset-Cheneau, D. Dolfi, R. Lebrun, P. Bortolotti, K. Belashchenko, S. Dhillon, H. Jaffrès, *Appl. Phys. Rev.* 7, 041409 (2020).

[15] M. E. Barnes, S. A. Berry, P. Gow, D. McBryde, G. J. Daniell, H. E. Beere, D.A. Ritchie, V. Apostolopoulos, *Opt. Express*, 21, 16263 (2013).

[16] E. Prieto, S. Vizcara, A. Somintac, A. Salvador, E. Estacio, C. Que, K. Yamamoto, M. Tani, *J. Opt. Soc. Am. B*, 31, 291 (2014).

[17] B. Guzelturk, M. Trigo, O. Delaire, DA. Reis, AM Lindenberg, *ACS Photonics*, 8, 3633 (2021).

[18] N. Goubet, A. Jagtap, C. Livache, B. Martinez, H. Portalès, X. Z. Xu, R. Lobo, P. S. M., B. Dubertret, E. Lhuillier, Terahertz *J. Am. Chem. Soc.*, 140, 15, 5033 (2018).

[19] G. Shen, M. Chen, P. Guyot-Sionnest, *J. Phys. Chem. Lett.*, 8, 2224 (2017).

[20] S. Pierini, F. Capitani, M. Scimeca, S. Kozlov, D. Pierucci, R. Alchaar, C. Abadie, A. Khalili, M. Cavallo, T. H. Dang, H. Zhang, E. Bossavit, C. Gréboval, J. Avila, B. Baptiste, S. Klotz, A. Sahu, C. Feuillet-Palma, X. Z. Xu, A. Ouerghi, S. Ithurria, J. K. Utterback, S. Sauvage, E. Lhuillier, *J. Phys. Chem. Lett.*, 13, 6919 (2022).

[21] A. Jagtap, C. Livache, B. Martinez, J. Qu, A. Chu, C. Gréboval, N. Goubet, E. Lhuillier, *Opt. Mater. Express*, 8, 1174 (2018).

[22] J. Kim, D. Choi, K. S. Jeong, *Chem. Commun.*, 54, 8435 (2018).

[23] T. Apretna, S. Massabeau, C. Gréboval, N. Goubet, J. Tignon, S. Dhillon, F. Carosella, R. Ferreira, E. Lhuillier, J. Mangeney, *Nanophotonics*, 10, 2753 (2021).

[24] M. Ruppert, H. Bui, L. K. Sagar, P. Geiregat, Z. Hens, G. Bester, N. Huse. *Nanoscale*, 14, 4123 (2022).

[25] Yu. B. Vasilyev, N. N. Mikhailov, G. Yu. Vasilyeva, Yu. L. Ivánov, A. O. Zakhar'in, A. V. Andrianov, L. E. Vorobiev, D. A. Firsov, M. N. Grigoriev, A. V. Antonov, A. V. Ikonnikov, and V. I. Gavrilenko, *Semiconductors*, 50, 915 (2016).

[26] S. V. Morozov, V. V. Rumyantsev, M. S. Zholudev, A. A. Dubinov, V. Ya. Aleshkin, V. V. Utochkin, M. A. Fadeev, K. E. Kudryavtsev, N N. Mikhailov, S. A. Dvoretskii, V. I. Gavrilenko, F. Teppe, *ACS Photonics*, 8, 3526–3535 (2021).

[27] P. Rastogi, A. Chu, T. H. Dang, Y. Prado, C. Gréboval, J. Qu, C. Dabard, A. Khalili, E. Dandeu, B. Fix, X. Z. Xu, S. Ithurria, G. Vincent, B. Gallas, E. Lhuillier, *Adv. Optical Mater.*, 9, 2002066 (2021).

[28] M. Baillergeau, K. Maussang, T. Nirrengarten, J. Palomo, L. H. Li, E. H. Linfield, A. G. Davies, S. Dhillon, J. Tignon, J. Mangeney, *Sci Rep*, 6, 24811 (2016).

[29] P. Hale, J. Madeo, C. Chin, S. Dhillon, J. Mangeney, J. Tignon, K. Dani, *Opt. Express*, 22, 26358 (2014).

[30] Philippe Guyot-Sionnest, *J. Phys. Chem. Lett.*, 3, 1169–1175 (2012).

[31] J. Gao, J., A. Fidler, A., V. Klimov, *Nat Commun* 6, 8185 (2015).

[32] S. D. Ganichev, W. Prettl, Oxford Univ. Press, 2006.

[33] J. W. McIver, D. Hsieh, H. Steinberg, P. Jarillo-Herrero, N. Gedik, *Nature Nanotech.*, 7, 96 (2012).

[34] H. Plank, J. Pernul, S. Gebert, S. N. Danilov, J. Konig-Otto, S. Winnerl, M. Lanius, J. Kampmeier, G. Mussler, I. Aguilera, D. Grutzmacher, S. D. Ganichev, *Phys. Rev. Materials*, 2, 024202 (2018).

[35] A. Bundulis, I. A. Shuklov, V. V. Kim, A. A. Mardini, J. Grube, J. Alnis, A. A. Lizunova, V. F. Razumov, R. A. Ganeev, *Nanomaterials*, 11, 3351 (2021).

[36] H. Plank, L. E. Golub, S. Bauer, V. V. Belkov, T. Herrmann, P. Olbrich, M. Eschbach, L. Plucinski, C. M. Schneider, J. Kampmeier, M. Lanius, G. Mussler, D. Grutzmacher, S. D. Ganichev, *Phys. Rev. B*, 93, 125434, (2016).

[37] C. Kastl, C. Karnetzky, H. Karl, A. W. Holleitner, *Nat Commun* 6, 6617 (2015).

[38] Q. Ma, S.-Y. Xu, C.-K. Chan, C.-L. Zhang, G. Chang, Y. Lin, W. Xie, T. Palacios, H. Lin, S. Jia, P. A. Lee, P. Jarillo-Herrero, N. Gedik, *Nature Phys* 13, 842–847 (2017)

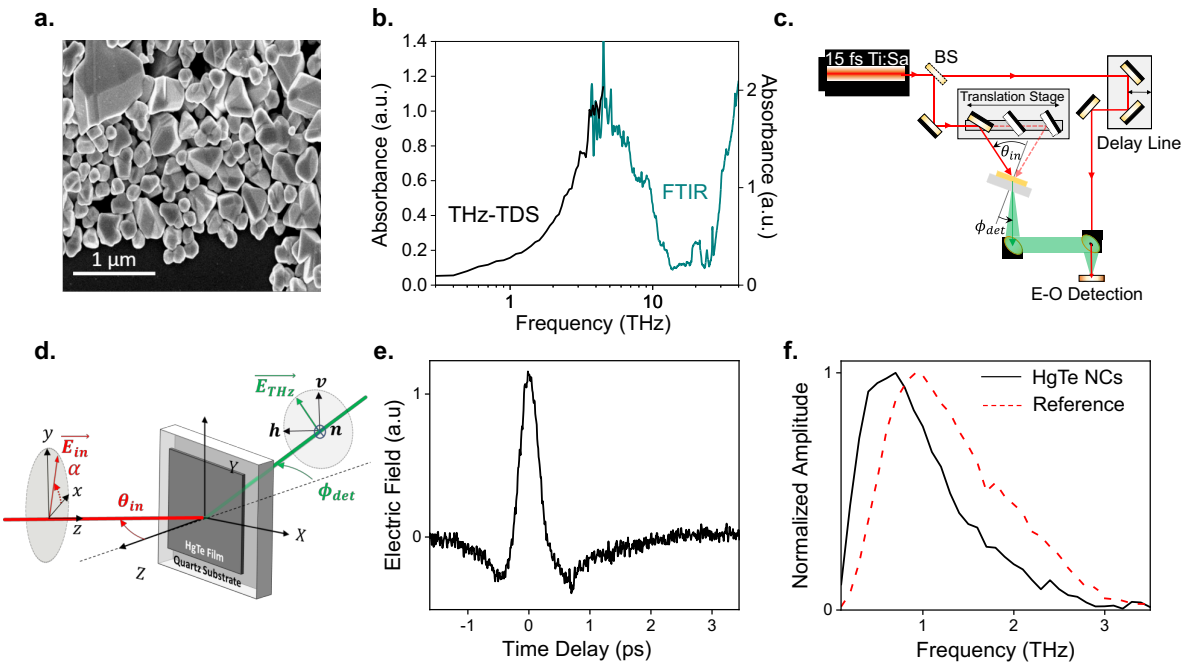
a.
1 µm
b.
Absorbance (a.u.)
Absorbance (a.u.)
THz-TDS
FTIR
Frequency (THz)
c.
15 fs Ti:Sa
BS
Translation Stage
Delay Line
E-O Detection
d.
HgTe Film
Quartz Substrate
e.
Electric Field (a.u)
Time Delay (ps)
f.
HgTe NCs
Reference
Normalized Amplitude
Frequency (THz)

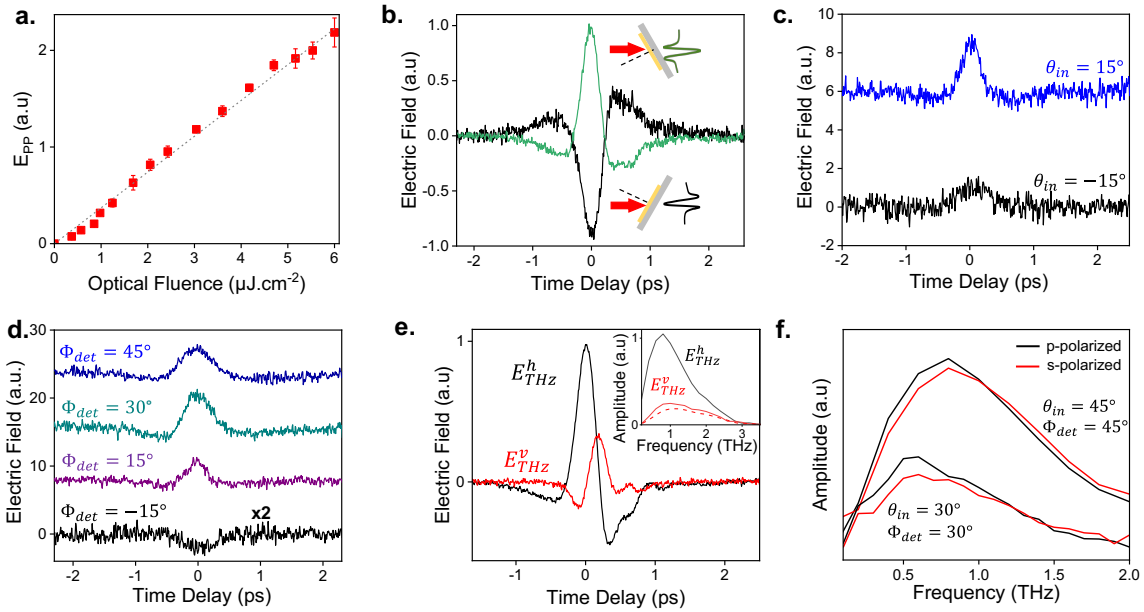
a.
E_{PP} (a.u)
Optical Fluence (μJ.cm^{-2})
b.
Electric Field (a.u)
Time Delay (ps)
c.
Electric Field (a.u.)
$\theta_{in} = 15°$
$\theta_{in} = -15°$
Time Delay (ps)
d.
Electric Field (a.u.)
$\Phi_{det} = 45°$
$\Phi_{det} = 30°$
$\Phi_{det} = 15°$
$\Phi_{det} = -15°$
x2
Time Delay (ps)
e.
Electric Field (a.u)
E^h_{THz}
E^v_{THz}
Amplitude (a.u)
Frequency (THz)
Time Delay (ps)
f.
Amplitude (a.u)
p-polarized
s-polarized
$\theta_{in} = 45°$
$\Phi_{det} = 45°$
$\theta_{in} = 30°$
$\Phi_{det} = 30°$
Frequency (THz)

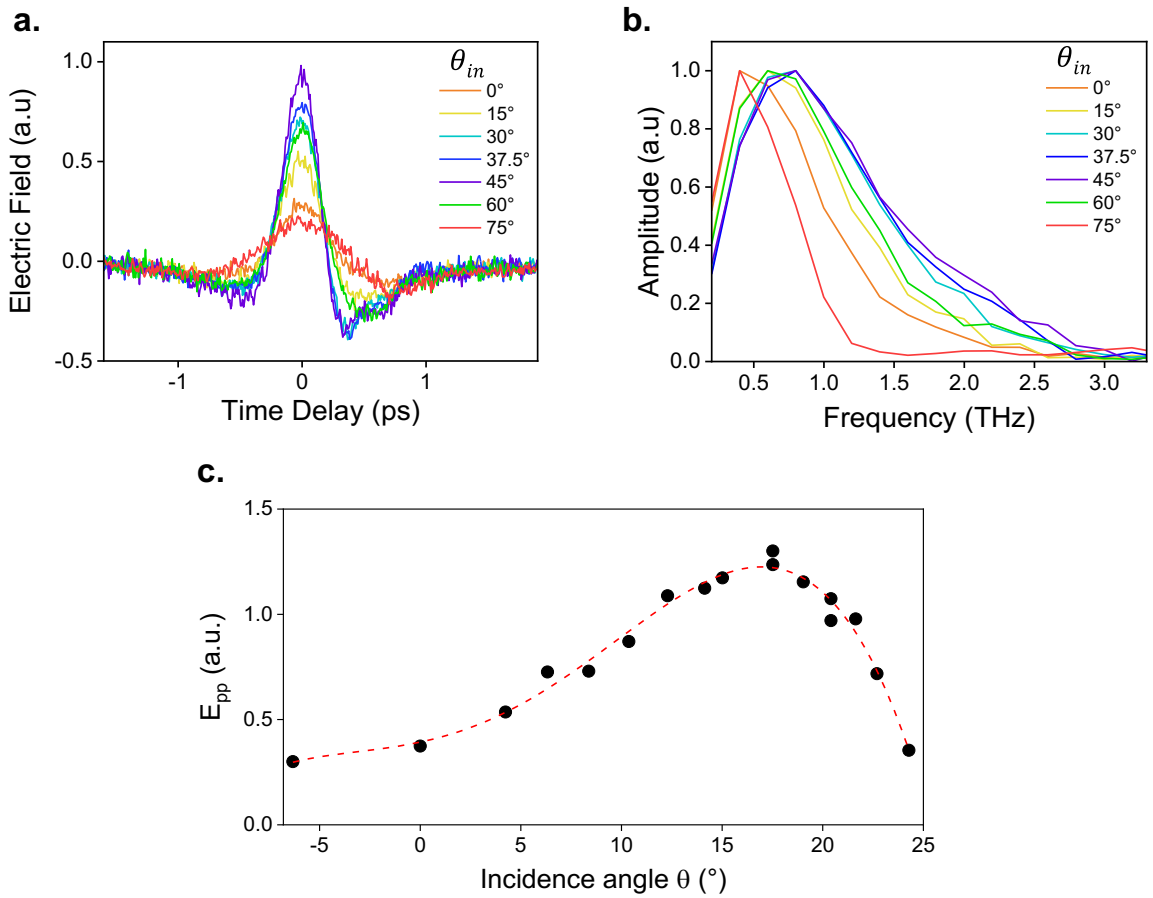
a.
Electric Field (a.u)
Time Delay (ps)
θ_{in}
0°
15°
30°
37.5°
45°
60°
75°
b.
Amplitude (a.u)
Frequency (THz)
c.
E_{pp} (a.u.)
Incidence angle θ (°)